Automatic determination of image quality parameters in digital radiographic imaging systems

Martin Brok and Cornelis H. Slump
Philips Medical Systems
P.O. box 10000 Best, The Netherlands

1 abstract

It is shown, that the Image Quality parameters, Modulation Transfer Function (*MTF*) and noise can be evaluated digitally with high accuracy. The systems *MTF* is measured by the use of a 5 slits phantom. Simulation studies are showing the optimal phantom dimension and indicate the expected precision of the measurement. By comparison studies with conventional techniques the *MTF* measurement procedure is validated for the effects of pixel coarseness, noise and limiting resolution.

An analytical expression for signal-to-noise ratio in a digital radiographic system is developed. Predicted values are compared with measured data.

2 introduction

Image Quality (IQ) is gaining more interest by those who are involved in X ray diagnostic imaging. One of the reasons of the increased attention to IQ are the improved abilities of the diagnostic systems with respect to acquisition and processing techniques. Due to image processing techniques as noise reduction and edge enhancements, system imperfections will be earlier noticeable in the image as before.

Until recently IQ was determined by visual inspection of images recorded from appropriate phantoms. The main disadvantage of this type of IQ judgement is the observer dependency and the limitations in quantifying the IQ parameters. To avoid these restrictions more objective measurements evaluated by the diagnostic system should replace the conventional observations whenever possible.

In the present paper the automatic evaluation of IQ is illustrated by two parameters. The first is the systems Modulation Transfer Function (*MTF*), which encloses the image intensifier, TV chain and the digital equipment. The second parameter is related to the systems noise.

3 modulation transfer function

The *MTF* of an imaging system is the modulus of the two dimensional Fourier transform of the point spread function. Because of the TV-target scanning the most relevant information is contained in the one dimensional videoline. Fortunately this limits the calculations to the one dimensional Fourier transform of the line spread function.

To control aliasing artifacts in the *MTF* measurement *Sones and Barnes* [1] proposed in 1984 a procedure based on a multi wire phantom which was able to measure the *MTF* even beyond the Nyquist frequency.

In 1985 *Fujita et al.* [2] presented a *MTF* measuring procedure for digital systems based on a single frame image of a slightly angulated slit. Fourier transforms of the line spread function were obtained from different alignments with respect to the pixel array in order to calculate the presampling analog *MTF*.

The latter method has the advantage of a very simple phantom, which is easy to construct. The main disadvantage is, however, the increase in cpu time in finding the proper alignments, specially when the data is noisy.

In this paper the basic ideas of *Sones and Barnes* [1] are used. Computer simulatuions have been used to optimize the phantom dimensions and comparison studies are described to validate the results.

3.1 theory

The *MTF* of a digital imaging system is calculated by the modulus of the discrete Fourier transform of the product of the Line Spread Function *LSF* and the sampling *comb* function.

$$MTF(\nu) = \mid \Delta x \sum_{k=0}^{N-1} \{LSF(x) \,.\, comb(k\Delta x) \,.\, e^{i2\pi\nu k\Delta x}\} \mid \tag{1}$$

Where N is the number of pixels describing the image line and ν is the frequency sampling of the *MTF*.

$$\nu = \frac{i}{N\Delta x}, \qquad i = 0, 1, 2, \ldots, N-1 \tag{2}$$

A *LSF* is usually found by imaging a small slit. The phantom considered here consists of 5 parallel equidistantial slits, as is schematically depicted in fig. 1.

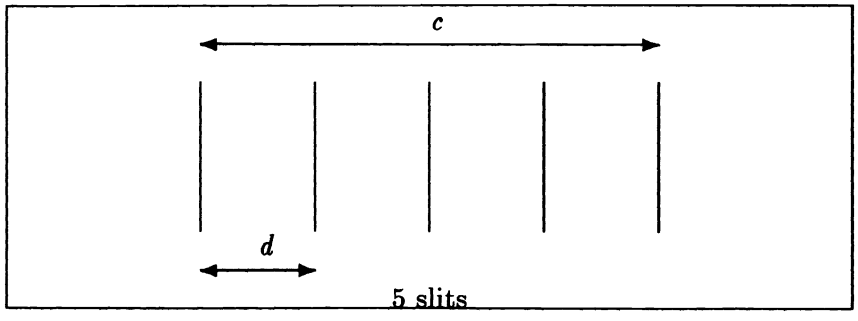

Figure 1: Schematic drawing of the multi-slit phantom.

The spatial dimensions of the imaged phantom is mathematically best described by a periodic train of *LSF's* which is limited by a rectangular function *rect(x/c)*. The periodicity is represented by a convolution with a spatial comb function *comb(x/d)* depending on the interslit distance d.

The Fourier transform of the imaged phantom *I(ν)* can be written as:

$$I(\nu) = \left| \Delta x \sum_{k=0}^{N-1} \{[LSF(x) * comb(x/d)] \,.\, rect(x/c) \,.\, comb(k\Delta x) \,.\, e^{i2\pi\nu k\Delta x}\} \right| \quad (3)$$

This equation can be rewritten as:

$$I(\nu) = \{(MTF(\nu) \,.\, comb(\nu d)) * sinc(\nu c)\} * comb(\nu_N) \quad (4)$$

From (4) we can deduce that the MTF is the envelope of a periodic train of sinc functions $comb(\nu d) * sinc(\nu c)$ repeating with the Nyquist frequency ν_N.

Due to the limited number of points describing the MTF envelope curve, this measuring procedure is not suitable to estimate the Low Frequency Drop LFD.

Johnson [3] and *Verhoeven* [4] pointed out that the MTF curve of an imaging system can be fitted by the expression:

$$MTF = e^{(\frac{\nu}{\nu_c})^n} \quad (5)$$

where ν_c is the frequency constant and n is called the "device index". In this paper various MTF curves are fitted with this equation and are extrapolated to the zero frequency.

3.2 simulation

Distortions in the image produced by an imaging system, such as pincushion, has its impact on the accuracy of the MTF measurement. To find out in what extend the distortion influences the MTF result, extensive computer simulations have been carried out. Two phantom design parameters (the number of slits and the interslit distance) were taken under investigation.

The two parameters are responsible for the overall phantom dimension. To reduce the effect of pincushion the phantom should be kept small with respect to the entrance screen of the image intensifier. One way to achieve this is to minimize the interslit distance. From eq. 4 we see that a decrease in the interslit distances will result in a increase in the sampling interval of the MTF frequency peaks. Because of their inverse relationship a compromise has to be the result.

The overall phantom dimension will determine the width of the peaks in the frequency domain, so by a given interslit distance the number of slits should be large enough to give a good separation of the individual peaks.

Simulations with the above mentioned phantom design parameters pointed out that with an interslit distance of 5 mm and a total number of 5 slits, the interpeak distance in the frequency domain is small enough to give a suitable set of points describing the MTF curve. Also the width of the frequency peaks are small compared to the interpeak distance.

A distortion in the mutual interslit distance was artificially introduced by a linear increase in the distance as is shown in fig. 2.

A measure for the relative error E is defined to be:

$$E = \frac{dev}{x} \,.\, 100\% \quad (6)$$

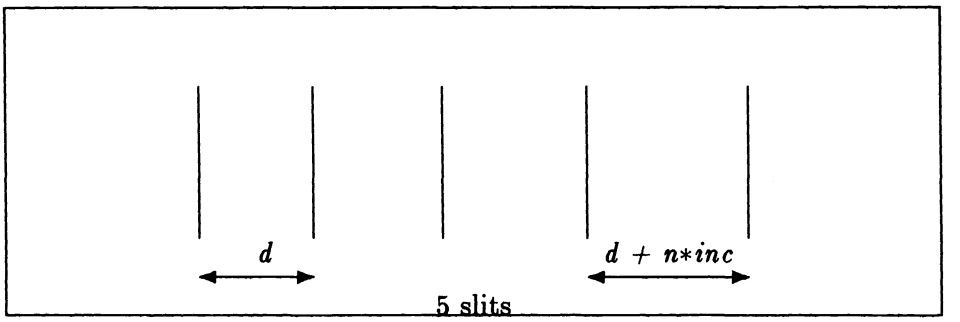

Figure 2: Distorted multi-slit image. d is the initial interslit distance and inc is the linear increment.

Where x is the average interslit distance and dev is the maximum deviation from x.

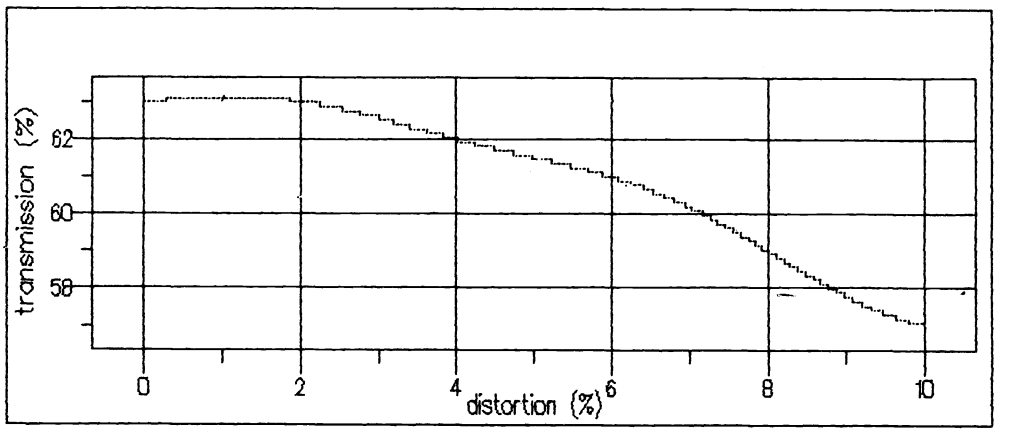

Figure 3: Plot of change in transmission value at half the Nyquist frequency against the introduced distortion in interslit distances.

We have calculated the MTF curves for distortions ranging from 0 to 10%. In fig. 3 the transmission values at half the Nyquist frequency are plotted against the introduced distortions. This plot shows that even with an introduced distortion of 6% the change in transmission value is less then 1%, which is for most cases acceptable.

3.3 results

To validate the MTF results obtained from the 5 slits phantom, several comparison studies have been carried out in which we investigated the following:

- The effect of coarseness of the pixelarray.
- The noise contribution to the MTF-curve.
- The maximum resolution determined from the MTF-curve with respect to the maximum resolution derived from bar patterns.

The equipment used for the measurements were engineering models of a Philips DVI (Digital Vascular Imaging) and DCI (Digital Cardiac Imaging). For high frequency sampling (up to 100 MHz) a Tektronix 2430A digital storage scope was used. All data were processed on a PC/AT compatible computer.

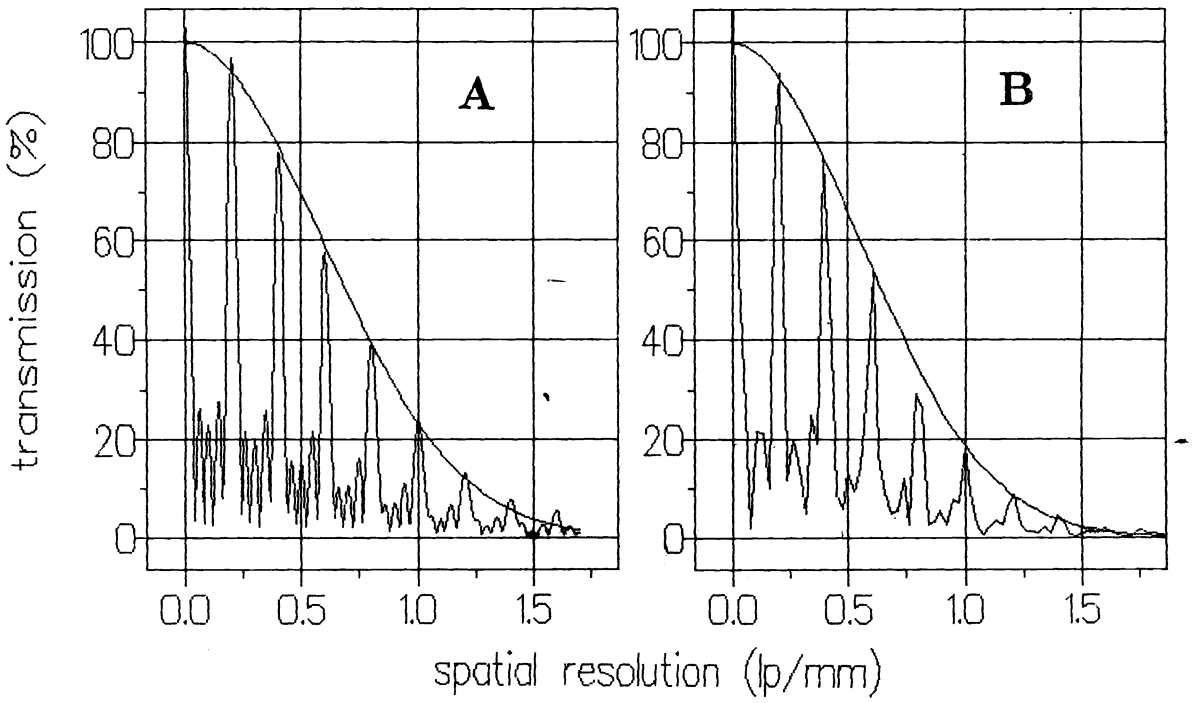

Figure 4: *MTF*'s obtained from an imaged multi-slit phantom at sampling frequencies of a) 12.5 MHz and b) 100MHz.

To compare the accuracy of the measurement with respect to the pixel dimension (sampling rate) an image of the multi-slit phantom was recorded with a DVI at high dose (1000 μR). At the same time an analog videoline perpendicular to the slits direction was digitized with the storage scope. Because of the eight times higher sampling frequency of the storage scope its internal frequency resolution will also be eight times higher, however, the spatial resolution will still be limited by the systems response. Differences in the frequency spectra of both measuring procedures can only be caused by their sampling frequency.

The density profiles as obtained from the DVI and Tektronix scope were first corrected for background by subtracting a quadratic interpolation of the midpoints between the slits. The resulting 5 nearly equidistantial *LSF's* superposed on a zero background level are succeedingly corrected for intensity changes, respecting the individual lineshapes.

The spatial pixel dimension can be calculated from the known interslit distance by counting the number of pixels between the slits. This gives us the opportunity to calculate the spatial frequencies in the plane of the phantom and from the known interslit distances the geometric distortion. With the aid of fig. 3 we are now in the fortunate situation to decide at forehand wether the *MTF* curve will have the desired accuracy.

In fig. 4 the *MTF*'s of the DVI and scope are shown as they were found by performing the Fourier transform on the corrected equidistantial *LSF's*. Apart from some minor changes in the spectra due to the number of points describing the spectra in the frequency domain the spectra are in good resemblance.

The effect of the noise contribution to the *MTF* has been measured by using a DCI with a typical dose rate of 10 μR per frame. In this case quantum noise is dominant to fixed-pattern and TV-chain noise. By calculating the *MTF* of the individual pixel rows out of the 512 x 512 multi-slit image the differences in the spectra are then reflected by the variation in the fit parameter ν_c from (5) assuming that the *MTF* curve is Gaussian ("device index " n = 2).

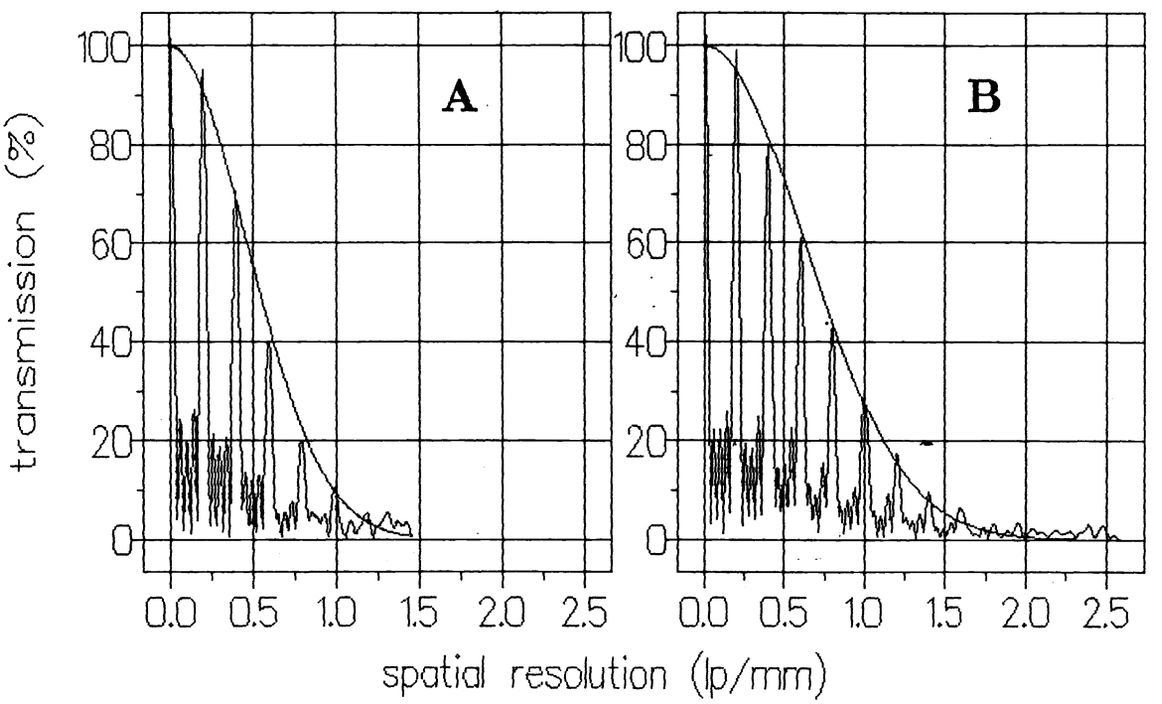

Figure 5: *MTF*'s obtained from an imaged multi-slit phantom recorded with a DCI at a) 9" mode and b) 5" mode.

The differences in ν_c found in the images were 2 - 5 %, depending on the Image Intensifier (II) mode (5", 6.5" and 9"). Although the variation in ν_c is relatively small, an improvement can be made by averaging the Fourier transforms of the adjacent pixel-rows to reduce the "noise" in the frequency domain.

Another approach to verify the multiline *MTF* method is by comparing the transmission value at 2% with the maximum resolution visable from bar patterns. For this study a DCI with a triple mode image intensifier has been used. At the 9" and 5" modes recordings has been made of the multislit phantom and at the same time the maximum resolution was obtained from an imaged resolution wedge phantom.

In fig. 5 the *MTF* curves are displayed. The corresponding maximum resolutions, viewed from the fan shaped phantom, were 1.2 - 1.3 *lp/mm* at 9" mode and 2.0 - 2.1 *lp/mm* at 5" mode. The maximum resolution at the 5" mode is in good agreement with the 2% transmission of the *MTF* curve. The results at 9" mode do not match as good as in the 5" mode. This is probably due to aliasing since the *MTF*

curve is not zero at the Nyquist frequency.

4 signal-to-noise ratio

The Image Quality of an II-TV based diagnostic image is not only ruled by its contrast and spatial resolution capability as expressed in the *MTF* but also by noise. We therefore seek to characterize the noise behaviour of a digital diagnostic imaging system . The modelling of the noise in such digital systems has been the subject of many papers, e.g. [5-14]. For the present discussion we will simplify things by only taking into account quantum noise and electrical noise.

Quantum noise is dependant of the input dose of the II and is furthermore influenced by the Detection Quantum Efficiency (DQE) and the *MTF* of the pertinent system. Electrical noise is mainly TV camera noise, e.g. shot-noise in the scanning electron beam, thermal noise of the load resistor and pre-amplifier noise.

In this contribution we characterize the system's noise behaviour by an expression for the signal-to-noise ratio in the detected digital image of a flat phantom e.g. 10 cm water. The predicted values for the signal-to-noise ratio based on the imaging parameters II input dose and *MTF* are compared with measurements. From this comparison conclusions will be drawn about the effectivity of the parameter "digital signal-to-noise ratio" in a quality assurance program.

4.1 theory

In this part of the paper random variables will be underlined. The number of X-ray photons $\underline{n}$ impinging on the II input screen per mm^2 are Poisson distributed, with the following probability distribution:

$$P\{\underline{n} = k\} = e^{-\lambda}\,\frac{\lambda^k}{k!} \qquad k = 0, 1, 2, \ldots. \tag{7}$$

with λ the average number of photons per mm^2. For simplicity we assume here that the photons all have the same effective energy. On the input screen the incoming photons form a uniformly distributed two-dimensional shot-noise process. We follow here the shot-noise analysis of *Papoulis* [15] (pp.560, 561). With $h(x, y)$ the point spread function characterizing the II-TV-digital system, we obtain for the output signal $\underline{s}$(x, y), neglecting electrical noise and digitization effects:

$$\underline{s}(x, y) = \eta c \sum_i h(x - x_i, y - y_i), \tag{8}$$

where x and y are spatial coordinates in the detected image and (x_i,y_i) denote the random points with uniform density λ on the input screen representing the detected photons. The DQE is denoted by η, the total detection gain is denoted by c.

By Campbell's theorem *Papoulis* [15] (p. 561) we have for the expectation value of the output signal and the variance, respectively:

$$E\{\underline{s}(x, y)\} = \lambda \eta c \int_{-\infty}^{\infty} \int_{-\infty}^{\infty} h(x, y)\,dx\,dy, \tag{9}$$

$$\sigma^2\{\underline{s}(x,y)\} = \lambda\eta c^2 \int_{-\infty}^{\infty}\int_{-\infty}^{\infty} h^2(x,y)dxdy, \tag{10}$$

For the signal-to-noise ratio we obtain

$$\frac{S}{N} = \{\frac{\lambda\eta}{\int_{-\infty}^{\infty}\int_{-\infty}^{\infty} h^2(x,y)dxdy}\}^{\frac{1}{2}}. \tag{11}$$

The double integral in the denominator can be replaced by a single integral under the assumption of a circular symmetric point spread function. This results in

$$\frac{S}{N} = \{\frac{\lambda\eta}{2\pi\int_0^{\infty} \nu MTF^2(\nu)d\nu}\}^{\frac{1}{2}}. \tag{12}$$

a similar formula is stated in *Beekmans et al.* [16] (formula 3).

As pointed out by *Barnes* [17], a more intuitive understanding of the physical factors affecting the signal-to-noise ratio can be obtained by introducing in (12) the effective noise sampling aperture A_e as defined by *Wagner* [6]:

$$A_e = [2\pi\int_0^{\infty} \nu MTF^2(\nu)d\nu]^{-1} \tag{13}$$

With (13) we arrive at the following expression for the signal-to-noise ratio:

$$\frac{S}{N} = \{\lambda\eta A_e\}^{\frac{1}{2}} \tag{14}$$

For an ideal imaging system i.e. with analog $MTF = 1$ so that only the pixel MTF remains, A_e in (14) reduces to the (pixel area)$^{-1}$. This can be seen as follows, assume a circular pixel with radius a , the pixel MTF then reads as:

$$MTF(\nu) = \frac{aJ_1(2\pi a\nu)}{\nu} \tag{15}$$

and for (13) we obtain:

$$A_e^{-1} = 2\pi a^2 \int_0^{\infty} \frac{J_1^2(2\pi a\nu)}{\nu} d\nu = 2\pi a^2. \tag{16}$$

A less ideal system MTF will improve the signal-to-noise ratio due to additional blurring, at the expense of resolution performance.

So far the discussion is for quantum noise only.

In the next section we will apply the formulas (13), (14) for digital cine imaging with a typical TV pick-up tube beam current of 200 nA. According to *Verhoeven* [13], in this case the camera pre-amplifier noise is the dominant electrical noise with a typical noise current of 1 nA RMS.

4.2 results

In order to verify the expressions (13) and (14) the following experiment was performed. Images with matrix size 512^2 and bitdepth 8 were acquired at a rate of 25 frames/s and stored with an engineering model of Philips' Digital Imaging (DCI) system. The II was a 9"/6.5" dual mode image intensifier, the TV camera pick-up tube was the 2" Plumbicon 45XQ (XTV6). In the 9" mode three dose levels were applied, 8, 16 and 32 μR/frame. The dose level in the 6.5" mode follows the dose rate in the 9" mode by a factor of 1.9 (= $(9/6.5)^2$).

The signal-to-noise ratio of the digital images is calculated from two consecutive images $I_1(i,j)$ and $I_2(i,j)$ which are selected from each run. In the central area of a selected frame a Region Of Interest (ROI) of $11 * 11$ pixels is defined. For the signal S we have

$$S = \frac{\frac{1}{2}}{121} \sum_i \sum_j I_1(i,j) + I_2(i,j), \tag{17}$$

and the noise N is calculated as follows

$$N = [\frac{\frac{1}{2}}{121^2 - 1} \sum_i \sum_j \{I_1(i,j) - I_2(i,j) - \bar{I}\}^2]^{\frac{1}{2}}, \tag{18}$$

with

$$\bar{I} = \frac{1}{121} \sum_i \sum_j I_1(i,j) - I_2(i,j). \tag{19}$$

The images are acquired with a X-ray generator setting of 75 kVp and a pulse width of 5 ms. A filter of 1.5 mm Cu is applied to the X-ray collimator. The dose is measured at the entrance plane of the II. The TV aperture is adjusted such to keep the average video level at a constant level.

In both the 9" and the 6.5" mode the MTF of the system is measured by the method described in section 3. The obtained results are fitted with the exponential function, yielding:

$$\begin{aligned} 9" \quad &: MTF(x) = e^{(\frac{x}{b})^2}, \qquad with \quad b = 0.78 \ lp/mm \\ 6.5" \quad &: MTF(x) = e^{(\frac{x}{b})^2}, \qquad with \quad b = 0.94 \ lp/mm. \end{aligned}$$

With a LFD of 20% we obtain with (13) and (20)

$$A_e = \{(1 - LFD)^2 \frac{\pi}{2} b^2\}^{-1}, \tag{20}$$

at an effective noise sampling aperture A_e of 1.63 for the 9" mode and 1.12 for the 6.5" mode. With the 75 kVp and 1.5 mm Cu we have an effective photon energy of 60 keV. For this energy there are $3.2 * 10^{14}$ quanta/m^2 per R. So λ is $3.2 * 10^2$ quanta/mm^2 per μR. With a DQE value η of 60% the signal-to-noise ratio can be predicted from (14). No grid was used in the experiment. The theoretical and measured values are compared in table I.

II format [inch]	dose [μR/frame]	$\frac{S}{N}$ measured	theory
6.5	16	55	57
	32	71	81
	64	88	114
9	8	51	50
	16	64	71
	32	98	100

Table I: Comparison of the measured and predicted signal-to-noise ratio, eqs. (17)-(19) vs. (13) - (14). The lowest indicated dose rates are typical values for the cardiac application in Europe.

At the lower dose rates the agreement between theory and experiment is satisfactory. For higher dose levels, especially in the 6.5" mode, the deviations are substantial. This could be due to the neglect of the electrical noise from the present analysis. At the higher dose rates the quantum noise is not longer dominant and the electrical noise becomes relatively more important.

5 conclusion

The automatic assesment of IQ parameters has been shown, by the aid of two parameters, to be feasible for digital radiographic imaging systems. The systems *MTF* measuring procedure has been validated by comparison studies with a high frequency digitizer and by conventional techniques such as the observation of bar patterns. It is shown that the multislit *MTF* measuring procedure is very accurate and in good agreement with the results obtained from bar patterns.

It is clear from the noise experiments that the electrical noise needs to be incorporated in the expression for signal-to-noise ratio. Further research in this direction is necessary. The many system parameters influencing the signal-to-noise ratio make it a strong candidate for a image quality assurance program. Furthermore its implementation on digital imaging systems is easy as the algorithm is very simple.

6 references

1. R.A. Sones and G.T Barnes, "A method to measure the *MTF* of digital x-ray systems," Med. Phys. 11(2), 166-171 (1984).

2. H. Fujita, K. Doi, and M.L. Giger, "Investigation of basic imaging properties in digital radiography. 5.*MTF*s of II-TV digital imaging systems," Med. Phys. 12(6), 713-720 (1985).

3. C.B. Johnson, "Classification of electron-optical device modulation transfer functions," Adv. E.E.P. 35, 579-584 (1972).

4. L.A.J. Verhoeven, Digital Subtraction Angiography, Thesis, Technical University Delft, 164-168 (1985).

5. O.H. Schade, "Evaluation of noisy images," Proc. SPIE 56, 107-114 (1975).

6. R.F. Wagner, "Toward a unified view of radiological imaging systems," Part II: Noisy images, Med. Phys. 4, 279-296 (1977).

7. R.A. Kruger, C.A. Mistretta, S.J. Riederer, "Physical and technical considerations of computerized fluoroscopy difference imaging," IEEE Trans. Nucl. Sci. NS-28, 205-212 (1981).

8. S.J. Riederer, F.A. DiBianca et al. "Performance characteristics of a digital fluorographic system," Proc. SPIE 273, 88-94 (1981).

9. H. Roehrig, S. Nudelman et al. "Photoelectronic imaging for radiology," IEEE Trans. Nucl. Sci. NS-28, 190-204 (1981).

10. P.O. Scheibe, A.J. Thomas, "Noise sources in digital fluography," Proc. SPIE 314, 202-209 (1981).

11. M. Lissak Giger, K. Doi, C.E. Metz, "Investigation of basic imaging properties in digital radiography. 2. Noise Wiener Spectrum," Med. Phys. 11, 797-805, 1984.

12. M. Lissak Giger, K. Doi, "Investigation of basic imaging properties in digital radiography. 3. Effect of pixel size on SNR and threshold contrast," Med. Phys. 12, 201-206 (1985).

13. L.A.J. Verhoeven, "DSA imaging: some physical and technical aspects," Medicamundi 30, 46-55 (1985).

14. M. Lissak Giger, K. Doi, H. Fujita, "Investigation of basic imaging properties in digital radiography. 7. Noise Wiener spectra of II-TV digital imaging systems," Med. Phys. 13, 131-138 (1986).

15. A. Papoulis, Probability, Random Variables and Stochastic Processes, McGraw Hill, New York (1965).

16. A.A.G. Beekmans, J.A. den Boer, J.W. Haarman, B. v.d. Eijk, "Quality control of image intensifiers," Proc. AAPM on Acceptance Testing, pp. 1-25 (1981).

17. G.T. Barnes, "Radiographic mottle: A comprehensive theory," Med. Phys. 9, 656-667 (1982).